(Received 22 November 2023, Accepted 18 January 2024, Scheduled 28 January 2024)

Analysis and Design of an S-CL Compensated WPT System with Dual-Type Output Function

Qingsong Sang[1], Yilin Wang[2], Lin Yang[2], and Xuebin Zhou[3, *]

[1] *Wanbei Economic and Technical School, Fuyang, China*
[2] *College of Electronic and Electrical Engineering, Henan Normal University, Xinxiang, China*
[3] *College of intelligent Manufacturing, Hunan University of Science and Engineering, Yongzhou, China*

ABSTRACT: Simultaneous realization of load-independent dual-type output, namely constant current output (CCO) and constant voltage output (CVO), is necessary in some wireless power transmission (WPT) application fields. Therefore, an S-CL compensated WPT system with dual-type output function is proposed in this paper. This proposed system consists of a two-coil loosely coupled transformer (LCT), which can avoid cross-coupling phenomena, a transmitter-side compensation capacitor, a receiver-side compensation capacitor, and a receiver-side compensation inductor. Meanwhile, the proposed system can achieve near zero-phase-angle (ZPA) and zero-voltage-switching (ZVS) operations, avoiding power losses caused by reactive circulation. In addition, the theoretical analysis of the system's constant voltage and constant current outputs are further elaborated in this paper, and a test prototype is fabricated to verify the rationality and implementability of the proposed WPT system.

1. INTRODUCTION

Wireless power transfer (WPT) is an efficient, convenient, safe, reliable technology of transmitting electrical power [1, 2]. It is generally divided into magnetic coupling [3], ultrasonic [4], electric field coupling [5], and electromagnetic radiation [6] in the energy transfer modes of WPT technology. Among them, magnetic coupling technology has been developed rapidly and begun to be widely used in real life [7], such as electric vehicles [8], robots [9, 10], electric bicycles [11], unmanned aerial vehicle [12], and biomedical implants [13].

Nowadays, with the development of WPT technology, WPT systems with dual-type output function are beginning to attract widespread attention. The constant current output (CCO) ports in the WPT systems with dual-type output function are used for battery charging [14–16], while the constant voltage output (CVO) ports are used to power the detection module. Due to the advantage of being able to power different types of devices at the same time, it is of great significance to design a practical WPT system with dual-type output function. Existing dual-output WPT systems are mainly implemented by using dual receivers. For example, [17] proposed a dual-receiver WPT system. The first receiving side of the system can achieve CCO while the second receiving side can achieve CVO. However, it requires that the mutual inductance between the transmitting coil and the second receiving coil be set small enough to avoid their cross-coupling, which limits the freedom of coil design. [18] proposed a dual receiving system based on single capacitive coupling wireless power transmission (SCC-WPT) technology, and the dual receiving system uses a three-plate compact coupler to achieve CCO and CVO, but it requires four passive components on the transmitting side, which increases the system manufacturing cost.

For some other dual-receiver systems, dual-type output can be theoretically achieved by changing the compensation structure of the receiver such as [19, 20], but the decoupling method between receivers must use a magnetic cancellation method or a circuit-based method. In addition, the authors in [21] proposed a method to achieve dual-type output, which enables energy to be transmitted sequentially through the repeater unit, and CCO and CVO can be performed according to odd-even rules. However, the design of such systems is often more complex than a dual-receiver WPT system, and the repeater units inevitably have parasitic resistances, which reduces the efficiency of the system.

In short, the above-mentioned systems have a common shortcoming, that is, the number of receiving coils needs to be consistent with the number of load devices, which will increase the cost and volume of the system when there are many load devices. Therefore, in order to overcome this shortcoming, this paper proposes an S-CL compensated WPT system with dual-type output function. The system only requires a two-coil loosely coupled transformer (LCT), a compensation inductor, and two compensation capacitors to achieve dual-type output. At the same time, the system can meet near zero-phase-angle (ZPA) operation and zero-voltage-switching (ZVS) operation during the entire charging process, avoiding power loss caused. Therefore, the proposed system is low cost, simple in structure, and practical.

* Corresponding author: Xuebin Zhou (zhouxuebin821025@huse.edu.cn).

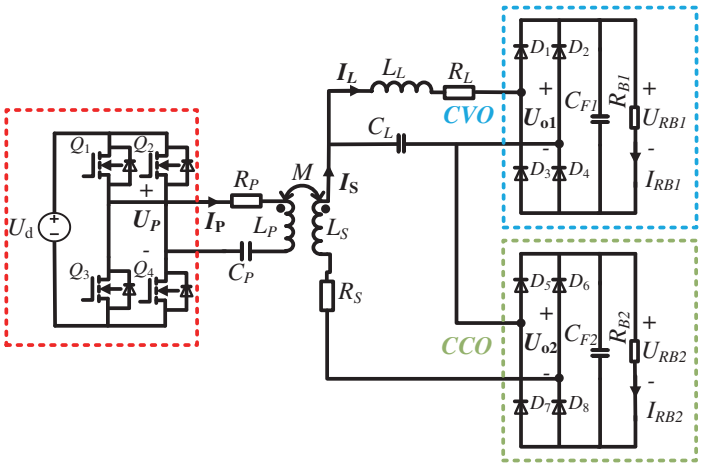

FIGURE 1. Circuit architecture of the proposed system with dual-type output.

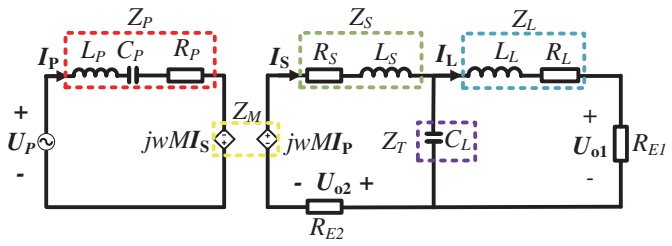

FIGURE 2. The equivalent circuit of the proposed system with dual-type output.

2. THEORETICAL ANALYSIS

2.1. Overview of an S-CL Compensated WPT System with Dual-Type Output Function

The circuit architecture diagram of the proposed S-CL compensated WPT system with dual-type output function is shown in Fig. 1. The transmitting side compensation tank of the system is composed of L_P, C_P, R_P, and the receiving side compensation tank of the system is composed of L_S, C_L, L_L, R_L, R_S. Among them, L_P and L_S are the self-inductances of the transmitting coil and receiving coil, respectively. C_L and C_S are the compensation capacitors on the receiving side and transmitting side, respectively. L_L is the compensation capacitor on the receiving side. R_P, R_S, and R_L are the parasitic resistances of the inductor coils L_P, L_S, and L_L, respectively, which can be ignored during specific analysis. M is the mutual inductor of loosely coupled transformer (LCT). Four diodes (D_1-D_4) form the rectifier of the receiving-side CVO port and four diodes (D_5-D_8) form the rectifier of the receiving-side CCO port. C_{F1} and C_{F2} are filter capacitors applied to the CVO port and CCO port, respectively. The root mean square value of the inverter's output AC voltage U_P and the input DC voltage U_d satisfy the following relationship.

$$U_P = \frac{2\sqrt{2}}{\pi} U_d \tag{1}$$

The equivalent circuit of the proposed system with dual-type output is displayed in Fig. 2. Among them, Z_P, Z_S, Z_T, Z_L, and Z_M indicate the equivalent impedance of the red box, green box, purple box, blue box, and yellow box, respectively. In order to facilitate theoretical derivation, the high-order harmonic components in the system circuit are ignored, then the expression of the above impedance can be expressed as

$$\begin{cases} Z_P = jX_P = j\left(\omega L_P - \dfrac{1}{\omega C_P}\right) \\ Z_S = jX_S = j(\omega L_S) \\ Z_T = jX_T = j\left(-\dfrac{1}{\omega C_L}\right) \\ Z_L = jX_L = j(\omega L_L) \\ Z_M = jX_M = j(\omega M) \end{cases} \tag{2}$$

R_{E1} represents the equivalent AC load resistance of the CVO port in the blue dotted box in Fig. 1, and R_{E2} represents the equivalent AC load resistance of the CCO port in the green dotted box in Fig. 1. The expressions of R_{E1} and R_{E2} are as follows.

$$R_{E1} = \frac{8R_{B1}}{\pi^2} \tag{3}$$

$$R_{E2} = \frac{8R_{B2}}{\pi^2} \tag{4}$$

According to Kirchhoff's voltage law (KVL), the matrix mathematical model of the proposed system can be expressed

as

$$\begin{bmatrix} \mathbf{U_P} \\ 0 \\ 0 \end{bmatrix} = \begin{bmatrix} Z_P & -Z_M & 0 \\ -Z_M & Z_S+Z_T+R_{E2} & -Z_T \\ 0 & -Z_T & Z_T+Z_L+R_{E1} \end{bmatrix} \begin{bmatrix} \mathbf{I_P} \\ \mathbf{I_S} \\ \mathbf{I_L} \end{bmatrix} \tag{5}$$

where $\mathbf{I_P}$, $\mathbf{I_S}$, and $\mathbf{I_L}$ are the current phasors flowing through L_P, L_S, and L_L, respectively. Then, substituting Eq. (2) into Eq. (5), the current phasors can be deduced as

$$\begin{cases} \mathbf{I_P} = \mathbf{U_P} \dfrac{-R_{E1}R_{E2}+X_LX_T+X_SB-jBR_{E2}-jCR_{E1}}{-X_M^2R_{E1}+X_PA-jX_M^2B} \\ \mathbf{I_S} = \mathbf{U_P} \dfrac{-X_MB-jX_MR_{E1}}{-X_M^2R_{E1}+X_PA-jX_M^2B} \\ \mathbf{I_L} = \mathbf{U_P} \dfrac{X_MX_T}{-X_M^2R_{E1}+X_PA-jX_M^2B} \end{cases} \tag{6}$$

where the symbols A, B, and C in Eq. (6) are expressed as follows:

$$\begin{cases} A = R_{E2}X_L+R_{E1}X_S+R_{E1}X_T+R_{E2}X_T \\ \quad +j(X_LX_T+X_SX_T+X_LX_S-R_{E1}R_{E2}) \\ B = X_L+X_T \\ C = X_T+X_S \end{cases} \tag{7}$$

2.2. Analysis of the CVO Characteristic

The voltage gain $E(\omega_{CV})$ at the CVO port is defined as the ratio of $\mathbf{U_{O1}}$ to $\mathbf{U_P}$, which can be obtained as

$$E(\omega_{CV}) = \left|\frac{\mathbf{U_{o1}}}{\mathbf{U_P}}\right| = \left|\frac{X_MX_TR_{E1}}{-X_M^2R_{E1}+X_PA-jX_M^2B}\right| \tag{8}$$

It is obvious from Eq. (8) that $E(\omega_{CV})$ is independent of the time-varying load when Eq. (8) satisfies the constraints shown in Eq. (9).

$$\begin{cases} X_P = 0 \\ B = X_L+X_T = 0 \end{cases} \tag{9}$$

According to Eq. (9), the voltage gain $E(\omega_{CV})$ can be simplified to

$$E(\omega_{CV}) = \left|\frac{\mathbf{U_{o1}}}{\mathbf{U_P}}\right| = \left|\frac{X_T}{-X_M}\right| \tag{10}$$

2.3. Overview of an S-CL Compensated WPT System with Dual-Type Output Function

According to Eq. (6) and Eq. (9), the current gain $G(\omega_{CC})$ at the CCO port is defined as

$$G(\omega_{CC}) = \left|\frac{\mathbf{I_S}}{\mathbf{U_P}}\right| = \left|\frac{j}{X_M}\right| \tag{11}$$

Based on Eq. (11), the second port can achieve CCO.

2.4. Analysis of the ZPA Operation

The total input impedance Z_{in} of the system is defined as the ratio of $\mathbf{U_P}$ to $\mathbf{I_P}$, which can be obtained by combining Eq. (6) and Eq. (9).

$$Z_{in} = \frac{\mathbf{U_P}}{\mathbf{I_P}} = \frac{-X_M^2R_{E1}}{-R_{E1}R_{E2}+X_LX_T-jCR_{E1}} \tag{12}$$

By observing Eq. (12), it is obvious that when $C = X_T+X_S = 0$ is hold, the equivalent input impedance of the system has only the real part, and therefore the system can achieve ZPA operation. Moreover, Eq. (12) for the input impedance of the system can be further simplified as

$$Z_{in} = \frac{\mathbf{U_P}}{\mathbf{I_P}} = \frac{-X_M^2R_{E1}}{-R_{E1}R_{E2}+X_LX_T} \tag{13}$$

3. PARAMETER DESIGN AND SIMULATION VERIFICATION

3.1. Parameter Design of the Proposed System

According to Eq. (9) and $C = X_T+X_S = 0$, C_P, C_L, and L_L can be derived as

$$\begin{cases} C_P = \dfrac{1}{\omega^2L_P} \\ C_L = \dfrac{1}{\omega^2L_S} \\ L_L = L_S \end{cases} \tag{14}$$

In Eq. (14), ω is the operating angular frequency, which is set to 85 kHz. The detailed parameter design process of the proposed WPT system is shown in Fig. 3. Further, Table 1 shows the relevant theoretical parameters of the proposed WPT system.

3.2. Verification of CVO Characteristic and CCO Characteristic under ZPA Operation

The curves of output voltage and related input impedance angle under different loads are shown in Fig. 4(a). It is clear that CVO and ZPA operation for variable loads can be achieved at a frequency point of 85 kHz. Fig. 4(b) shows the output current and related input impedance angle of the system under different loads. From Fig. 4(b), it can be noted that at the 85 kHz frequency point, both the CCO and ZPA operations of the system can be achieved for varying loads.

As evident from Figs. 4(a), (b), it can be concluded that the proposed system can simultaneously maintain CVO and CCO while satisfying ZPA operation.

3.3. Verification of ZVS Operation

According to Eq. (6), the input impedance of the system can be obtained as

$$Z_{in} = \frac{X_M^2R_{E1}-X_PA+jX_M^2B}{R_{E1}R_{E2}-X_LX_T-X_SB+jBR_{E2}+jCR_{E1}} \tag{15}$$

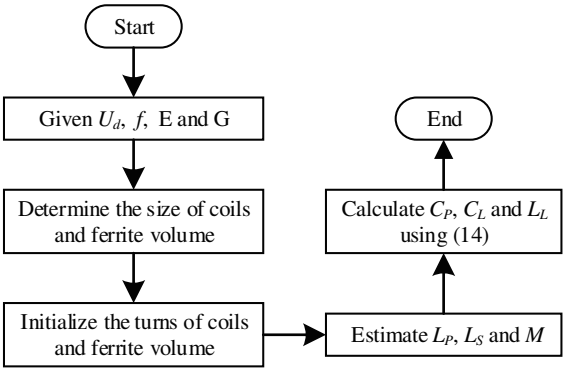

FIGURE 3. The detailed parameter design process of the proposed WPT system.

TABLE 1. The relevant theoretical parameters of the proposed WPT system.

Parameters	Value	Parameters	Value
U_d	50 V	C_L	70.01 nF
L_P	100 μH	L_L	49.6 μH
L_S	50 μH	C_P	34.99 nF
M	25 μH	f	85 kHz

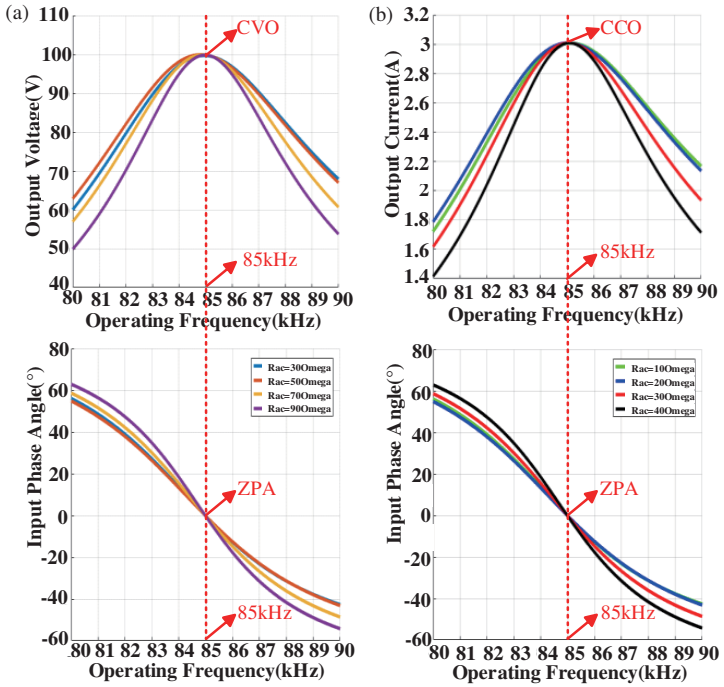

FIGURE 4. The curves of $E(\omega_{CV})$ and $G(\omega_{CC})$ and the related input impedance angle at different loads. (a) $E(\omega_{CV})$. (b) $G(\omega_{CC})$.

Input impedance angle β_{in} can be derived as

$$\beta_{in} = \arctan\left(\frac{(R_{E1}R_{E2} - X_L X_T - X_S B)X_M^2 B + (X_M^2 R_{E1} - X_P A)(BR_{E2} + CR_{E1})}{(R_{E1}R_{E2} - X_L X_T - X_S B)(X_M^2 R_{E1} - X_P A) + (BR_{E2} + CR_{E1})X_M^2 B}\right) \tag{16}$$

In order to more intuitively express the relationship with the input impedance angle under different loads, C_P, C_L, and L_L are normalized. It can be seen from Figs. 5(a), (b), and (c) that when C_P, C_L, and L_L increase or decrease appropriately, the

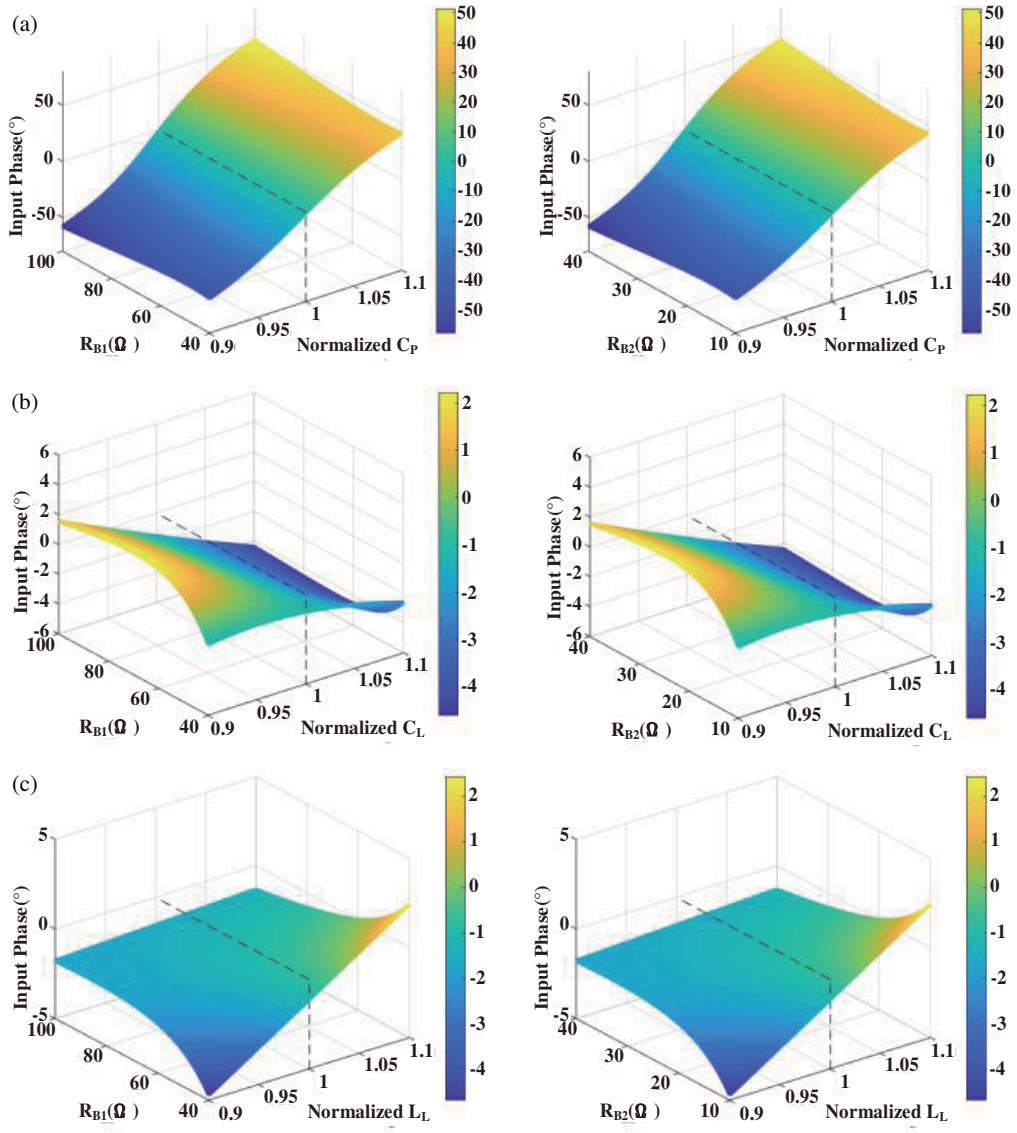

FIGURE 5. Input impedance angle β_{in} versus R_{B1} and R_{B2}, and normalized compensation element (a) C_P, (b) C_L, (c) L_L.

total input impedance of the system will appear weakly inductive, and this weak inductance will neutralize the influence of parasitic capacitance in the Metal-Oxide-Semiconductor Field Effect Transistors (MOSFETs), so that the system can achieve ZVS, thereby improving system efficiency.

By observing Fig. 6(c), it can be found that when only the compensation inductor L_L is changed, the changes in the output voltage and output current of the system are basically negligible. Therefore, by fine-tuning L_L, not only can the system operate in the ZVS state, but the system can still maintain the original CCO and CVO characteristics.

4. EXPERIMENTAL VERIFICATION

In order to further verify the correctness and practicability of the proposed method, a confirmatory experimental prototype is built as shown in Fig. 7. The experimental circuit parameters of the proposed WPT system are listed in Table 2. It is specified that the DC voltage source U_d is 50 V; the voltage of the CVO port is 100 V; and the current of the CCO port is 3 A. The WPT system with dual-type output in this paper can realize the CVO and CCO simultaneously through its inherent structural characteristics, without the need of complex control technology.

Figure 8 shows the relevant experimental waveforms of the proposed WPT system with dual-type output function. To be more convincing, an oscilloscope was used to capture the waveforms of the input voltage $\mathbf{U_P}$, input current $\mathbf{I_P}$, output voltage U_{RB1} of the CVO port, and the output current I_{RB2} of the CCO port under two sets of different loads. It can be seen from Fig. 8(a) that when the load resistance of the CVO port is 50 Ω, and the load resistance of the CCO port is 5 Ω, the system can achieve a CVO of 100 V and a CCO of 3 A. Based on Fig. 8(b), when the resistances of the CVO port and the CCO port are 100 Ω and 10 Ω, respectively, the two output ports of the proposed system can still maintain a CVO of 100 V and 3 A CCO, respectively. Obviously, under different load resistance condi-

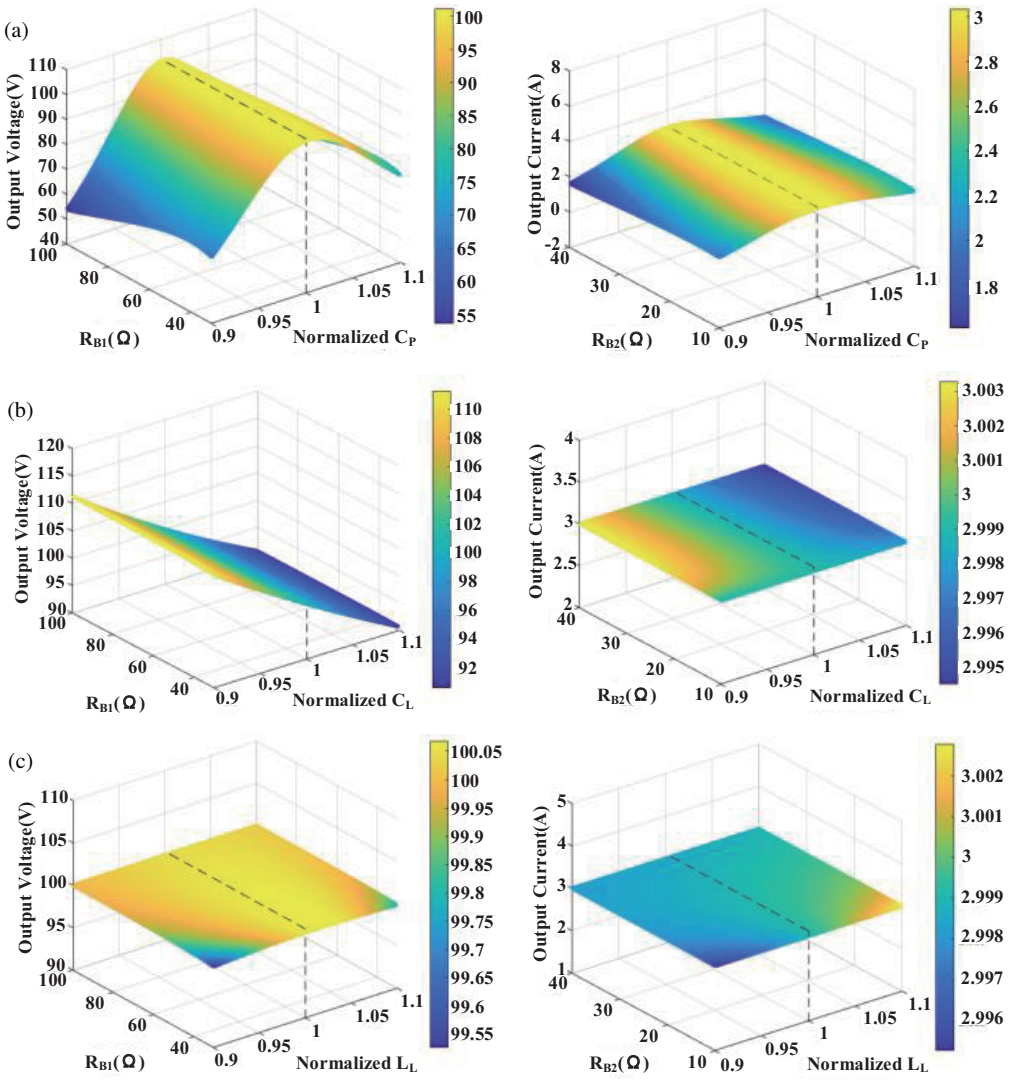

FIGURE 6. Output voltage versus R_{B1} and Output current versus R_{B2}, and normalized compensation element (a) C_P, (b) C_L, (c) L_L.

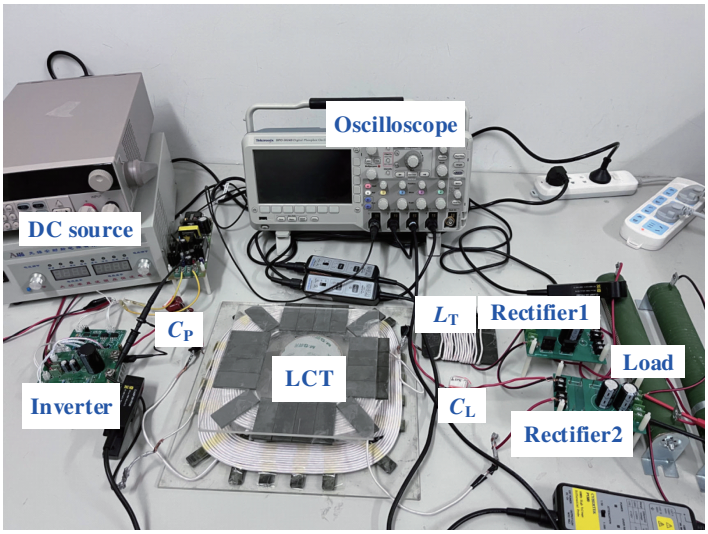

FIGURE 7. Laboratory setup of the proposed system.

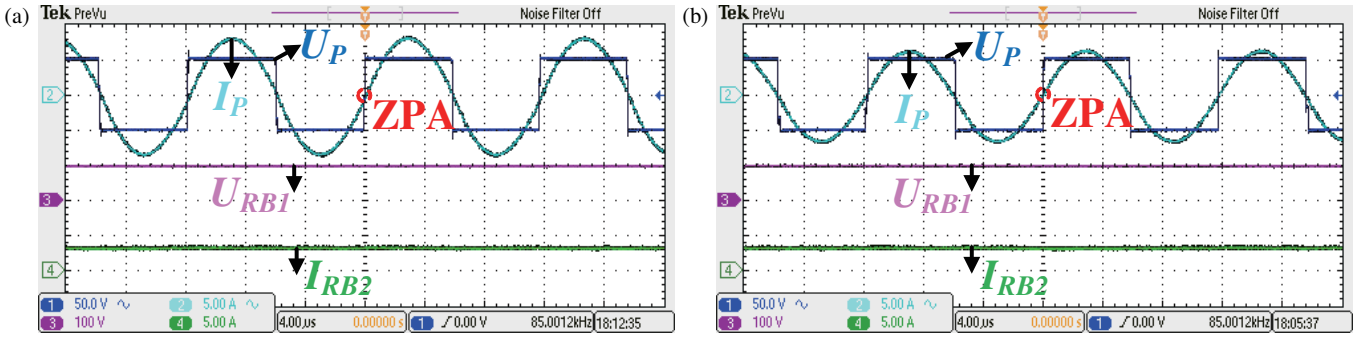

FIGURE 8. Experimental waveforms of $\mathbf{U_P}$, $\mathbf{I_P}$, U_{RB1} and I_{RB2} under ZPA condition when R_{B1} and R_{B2} are (a) 50 Ω, 5 Ω, (b) 100 Ω, 10 Ω, respectively.

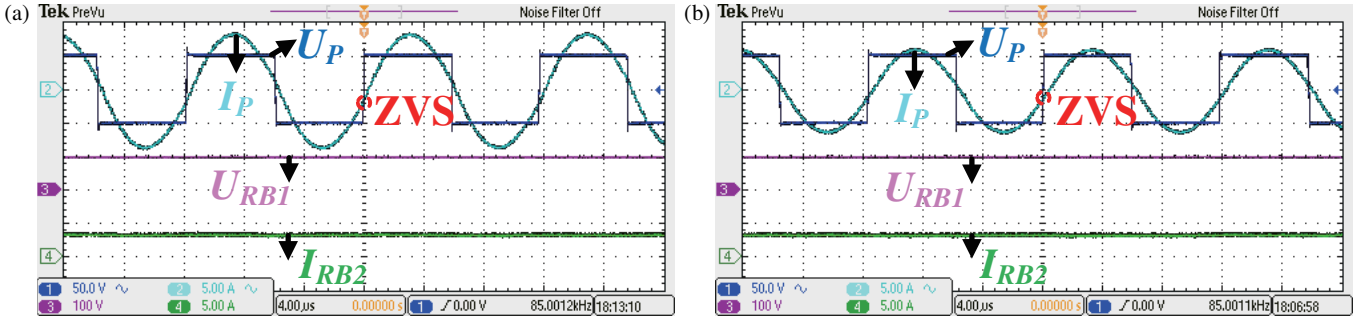

FIGURE 9. Experimental waveforms of $\mathbf{U_P}$, $\mathbf{I_P}$, U_{RB1} and I_{RB2} under ZVS condition when R_{B1} and R_{B2} are (a) 50 Ω, 5 Ω, (b) 100 Ω, 10 Ω, respectively.

TABLE 2. The experimental circuit parameters of the proposed WPT system.

Parameters	Value	Parameters	Value
U_d	50 V	C_L	70.06 nF
L_P	100.1 µH	L_L	49.3 µH
L_S	50.07 µH	$L_{L\text{-}ZVS}$	53.6 µH
M	25 µH	R_P	0.12 Ω
C_P	34.87 nF	R_S	0.06 Ω
f	85 kHz	R_L	0.06 Ω

tions, the output voltage of the CVO port and the output current of CCO port can maintain constant 100 V and 3 A, respectively. In addition, the input voltage $\mathbf{U_P}$ and input current $\mathbf{I_P}$ of the system always maintain the same phase when the load changes, which means that ZPA operation is achieved. In other words, the proposed dual-type output WPT system can achieve CVO, CCO, and ZPA operation.

When the compensation inductor of the secondary side is adjusted to $L_{L\text{-}ZVS}$ (53.6 µH), the load resistance R_{B1} of the CVO port and the load resistance R_{B2} of the CCO port are 50 Ω, 5 Ω, and 100 Ω, 10 Ω, respectively, and the experimental waveforms of $\mathbf{U_P}$, $\mathbf{I_P}$, U_{RB1}, and I_{RB2} are shown in Fig. 9. It can be seen that the input voltage $\mathbf{U_P}$ vector slightly exceeds the input current $\mathbf{I_P}$ vector, which means that adjusting L_L successfully achieves ZVS operation. In addition, when the load resistance changes, the system can maintain an output voltage U_{RB1} of 100 V and an output current I_{RB2} of 3 A under ZVS operation. This shows that the implementation of ZVS operation has no impact on the CVO characteristic and CCO characteristic.

Transient results with R_{B2} step change from 5 Ω to 10 Ω in CCO port and R_{B1} step change from 50 Ω to 100 Ω in CVO port are tested, as shown in Fig. 10. From Fig. 10, when both R_{B1} and R_{B2} are suddenly increased by 100%, the resulting changes in both charging current I_{RB2} in CCO port and the charging voltage U_{RB1} in CVO port are very small. In addition, there is no significant overshoot when R_{B1} and R_{B2} are changed suddenly. This further validates that the proposed system can perform dual-type output function stably.

Figure 11 shows the DC-DC experimental efficiency profiles of the CVO port when the CCO port is short-circuited and the CCO port when the CVO port is open circuit, respectively. As evident from Fig. 11, when the CCO port is short-circuited, the

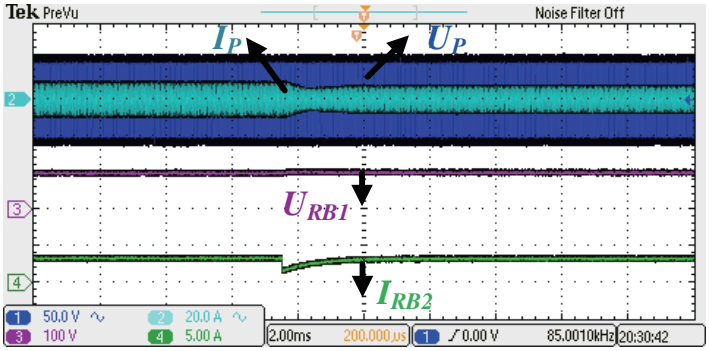

FIGURE 10. Transient results with R_{B2} step changes from 5 Ω to 10 Ω in CCO port and R_{B1} step changes from 50 Ω to 100 Ω in CVO port.

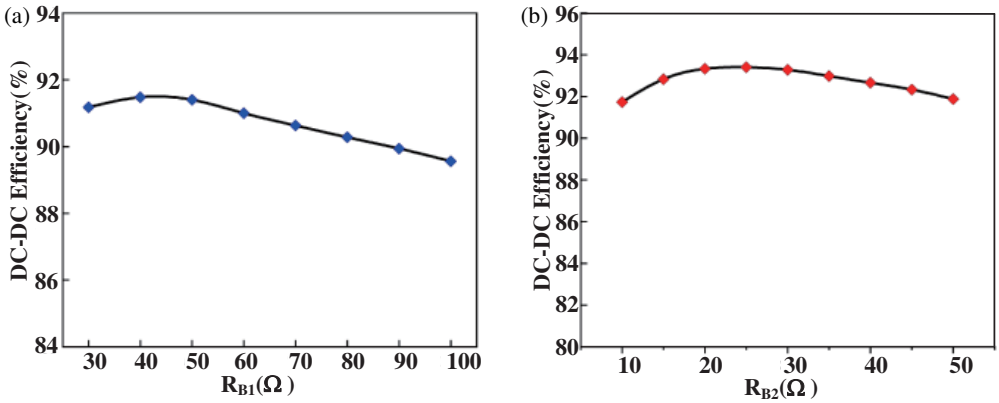

FIGURE 11. The DC-DC experimental efficiency of (a) the CVO port when the CCO port is short-circuited and (b) the CCO port when the CVO port is open circuit.

TABLE 3. Comparison of this work with other related studies.

Proposed in	Ref. [17]	Ref. [18]	Ref. [19]	Ref. [20]	Ref. [21]	This work
Power transfer method	Inductive	Capacitive	Inductive	Inductive	Inductive	Inductive
Number of coils or capacitor plates	3	5	4	3	4	2
Number of compensation components	3	8	4	6	4	3
Complex decoupling methods	No	No	Yes	Yes	Yes	No
Operating frequency (kHz)	200	1970	85	85	200	85
Output characteristics	CVO/CCO	CVO/CCO	Dual-CVO	Dual-CVO	CVO/CCO	CVO/CCO

maximum CVO efficiency can reach 91.48%. When the CVO port is open circuit, the maximum efficiency of the CCO can reach 93.4%. The overall DC-DC efficiency of the proposed system is always maintained at a high level.

In order to further demonstrate the advantages of the proposed system, a comparison was made between the proposed method and existing methods of the same type. The comparison results are listed in Table 3. As evident from Table 3, the proposed system in our paper does not require complex decoupling circuits, which is superior to the systems in [19–21]. In addition, compared to the systems in [17–21], the proposed system has fewer number of passive components, which has the advantages in terms of simple structure and low cost.

5. CONCLUSION

This paper proposes an S-CL compensated WPT system with dual-type output function. The system can achieve CVO, CCO, and near-ZPA operation under different load conditions. Meanwhile, the system can easily achieve ZVS operation by fine-tuning the secondary side compensation inductor to further improve the overall efficiency. Furthermore, fine-tuning the compensation inductor on the secondary side has a weak impact on the CVO and CCO functions of the proposed system. It is worth mentioning that this system only requires one dual-coil LCT and three passive components, which has great advantages in structure and economy. Finally, the correctness of the proposed system was verified by building an experimental prototype.

REFERENCES

[1] Yang, H., Y. Xu, Y. Gu, C. Zhu, J. Yu, R. Mai, Y. Li, Z. He, and U. K. Madawala, "Efficiency analysis and optimization method of power-relay IPT systems for reefer containers," *IEEE Transactions on Power Electronics*, Vol. 36, No. 5, 4942–4947, May 2021.

[2] Zhou, S. and C. C. Mi, "Multi-paralleled LCC reactive power compensation networks and their tuning method for electric vehicle dynamic wireless charging," *IEEE Transactions on Industrial Electronics*, Vol. 63, No. 10, 6546–6556, 2016.

[3] Yao, Y., Y. Wang, X. Liu, Y. Pei, and D. Xu, "A novel unsymmetrical coupling structure based on concentrated magnetic flux for high-misalignment IPT applications," *IEEE Transactions on Power Electronics*, Vol. 34, No. 4, 3110–3123, 2019.

[4] Meng, M. and M. Kiani, "Design and optimization of ultrasonic wireless power transmission links for millimeter-sized biomedical implants," *IEEE Transactions on Biomedical Circuits and Systems*, Vol. 11, No. 1, 98–107, 2017.

[5] Lian, J. and X. Qu, "An LCLC-LC-compensated capacitive power transferred battery charger with near-unity power factor and configurable charging profile," *IEEE Transactions on Industry Applications*, Vol. 58, No. 1, 1053–1060, 2022.

[6] Sadiq, B. O., A. A. Olaniyan, A. A. Ibrahim, and O. S. Zakariyya, "Li-Fi: The future propagation of wireless power transfer in vehicular AD HOC networks," in *2020 International Congress on Human-Computer Interaction, Optimization and Robotic Applications (HORA)*, 1–4, Ankara, Turkey, Jun. 2020.

[7] Kim, J. H., B.-S. Lee, J.-H. Lee, S.-H. Lee, C.-B. Park, S.-M. Jung, S.-G. Lee, K.-P. Yi, and J. Baek, "Development of 1-MW inductive power transfer system for a high-speed train," *IEEE Transactions on Industrial Electronics*, Vol. 62, No. 10, 6242–6250, Oct. 2015.

[8] Jiang, Y., L. Wang, Y. Wang, J. Liu, X. Li, and G. Ning, "Analysis, design, and implementation of accurate ZVS angle control for EV battery charging in wireless high-power transfer," *IEEE Transactions on Industrial Electronics*, Vol. 66, No. 5, 4075–4085, 2019.

[9] Sarin, A. and A.-T. Avestruz, "Code division multiple access wireless power transfer for energy sharing in heterogenous robot swarms," *IEEE Access*, Vol. 8, 132 121–132 133, 2020.

[10] Beh, H. Z. Z., G. A. Covic, and J. T. Boys, "Investigation of magnetic couplers in bicycle kickstands for wireless charging of electric bicycles," *IEEE Journal of Emerging and Selected Topics in Power Electronics*, Vol. 3, No. 1, 87–100, Mar. 2015.

[11] Wang, H., K. W. E. Cheng, and Y. Yang, "A new resonator design for wireless battery charging systems of electric bicycles," *IEEE Journal of Emerging and Selected Topics in Power Electronics*, Vol. 10, No. 5, 6009–6019, Oct. 2022.

[12] Cai, C., J. Wang, F. Zhang, X. Liu, P. Zhang, and Y.-G. Zhou, "A multichannel wireless UAV charging system with compact receivers for improving transmission stability and capacity," *IEEE Systems Journal*, Vol. 16, No. 1, 997–1008, Mar. 2022.

[13] Xiao, C., D. Cheng, and K. Wei, "An LCC-C compensated wireless charging system for implantable cardiac pacemakers: Theory, experiment, and safety evaluation," *IEEE Transactions on Power Electronics*, Vol. 33, No. 6, 4894–4905, Jun. 2018.

[14] Cai, C., J. Wang, M. Saeedifard, P. Zhang, R. Chen, and J. Zhang, "Gyrator-gain variable WPT topology for MC-unconstrained CC output customization using simplified capacitance tuning," *IEEE Transactions on Industrial Electronics*, Vol. 71, No. 4, 3594–3605, Apr. 2024.

[15] Yang, L., S. Jiang, C. Wang, Y. Shi, M. Wang, C. Cai, and L. Zhang, "A high-efficiency integrated LCC/S WPT system with constant current output," *IEEE Journal of Emerging and Selected Topics in Power Electronics*, 2023.

[16] Yuan, Z., M. Saeedifard, C. Cai, Q. Yang, P. Zhang, and H. Lin, "A misalignment tolerant design for a dual-coupled LCC-S-compensated WPT system with load-independent CC output," *IEEE Transactions on Power Electronics*, Vol. 37, No. 6, 7480–7492, Jun. 2022.

[17] Wang, H. and K. W. E. Cheng, "A dual-receiver inductive charging system for automated guided vehicles," *IEEE Transactions on Magnetics*, Vol. 58, No. 8, 1–5, Aug. 2022.

[18] Liu, Z., H. Hu, Y. Su, Y. Sun, F. Chen, and P. Deng, "A double-receiver compact SCC-WPT system with CV/CC output for mobile devices charging/supply," *IEEE Transactions on Power Electronics*, Vol. 38, No. 7, 9230–9245, 2023.

[19] Wang, H. and K. W. E. Cheng, "Analysis, design, and validation of a decoupled double-receiver wireless power transfer system with constant voltage outputs for industrial power supplies," *IEEE Transactions on Industrial Informatics*, Vol. 19, No. 1, 362–370, Jan. 2023.

[20] Mai, R., Y. Luo, B. Yang, Y. Song, S. Liu, and Z. He, "Decoupling circuit for automated guided vehicles IPT charging systems with dual receivers," *IEEE Transactions on Power Electronics*, Vol. 35, No. 7, 6652–6657, Jul. 2020.

[21] Zhou, Z., Z. Deng, C. Cheng, W. Li, F. Li, and C. Mi, "A wireless power transfer system with multiple constant current and constant voltage outputs," in *2019 IEEE Energy Conversion Congress and Exposition (ECCE)*, Baltimore, MD, USA, Sep. 2019.